Proton-Coupled Electron Transfer in DNA−Acrylamide Complexes†

Claudio Carra, Nedialka Iordanova, and Sharon Hammes-Schiffer*

Department of Chemistry, 152 Davey Laboratory, The Pennsylvania State University, University Park, Pennsylvania 16802

Received: April 9, 2002; In Final Form: May 29, 2002

A theoretical study of proton-coupled electron transfer (PCET) in the radical anionic thymine−acrylamide complex is presented. This study is based on a multistate continuum theory, in which the solute is represented by a multistate valence bond model, the solvent is described by a dielectric continuum, and the transferring hydrogen nucleus is represented by a quantum mechanical wave function. In this application, the ground and excited electronic states are calculated with the complete active space self-consistent-field (CASSCF) method, the electronic coupling for the electron transfer reaction is calculated with the generalized Mulliken−Hush method, and the solvation properties are calculated with the frequency-resolved cavity model. The influence of neighboring DNA base pairs is determined by studying solvated DNA−acrylamide models in addition to the solvated thymine−acrylamide complex. The calculations indicate that the final product corresponds to single electron transfer (ET) for the solvated thymine−acrylamide complex but to a net PCET reaction for the solvated DNA−acrylamide complex. This difference is due to a decrease in solvent accessibility in the presence of DNA, which alters the relative free energies of the ET and PCET product states. Thus, the balance between ET and PCET in the DNA−acrylamide system is highly sensitive to the solvation properties of the system.

I. Introduction

Proton-coupled electron transfer (PCET) reactions are thought to play an important role in electron and hole transfer in DNA. Experiments by Steenken suggest that interstrand proton transfer could interrupt the migration of electrons and holes in DNA by the conversion of radical ions to neutral radicals.[1,2] Further evidence of the importance of PCET in DNA is that a deuterium kinetic isotope effect has been observed for the electron transfer reactions of guanine in mononucleotides, single-stranded DNA,[3,4] and more recently duplex DNA.[5] Specifically, the rate of guanine oxidation is approximately 2 times larger in H_2O than in D_2O for these types of systems.[4,5] Theoretical studies by Sevilla and co-workers provide additional confirmation of the relevance of PCET reactions in DNA.[6−8]

Both experimental and theoretical results imply that PCET may occur in the DNA−acrylamide complex.[7,9] Radiation experiments indicate that the formation of the acrylamide anion radical is accompanied by protonation in solution.[10] In addition, acrylamide is known to be able to hydrogen bond to thymine by displacing adenine in DNA.[11] Furthermore, electron spin resonance (ESR) experiments on irradiated DNA−acrylamide complexes provide evidence for a thermally induced electron transfer from DNA to acrylamide at 130 K.[7,9] Motivated by these experiments, recently Sevilla and co-workers used density functional theory (DFT) to investigate the PCET reaction within a negatively charged thymine−acrylamide complex.[7] This PCET reaction is illustrated in Figure 1. They found that the unpaired spin density is delocalized over both thymine and acrylamide when the proton is bonded to thymine but the unpaired spin density becomes localized on acrylamide when the proton transfers to acrylamide. This result is interpreted as an indication that the proton transfer from thymine to acrylamide assists the electron transfer process from thymine to acrylamide.

In this paper, we apply a multistate continuum theory for PCET[12−15] to the same radical anionic thymine−acrylamide complex. In this theory, the solute is represented by a multistate valence bond model, the solvent is described by a dielectric continuum, and the transferring hydrogen nucleus is represented by a quantum mechanical wave function. In the application to the thymine−acrylamide complex, the ground and excited electronic states are calculated with the multiconfigurational complete active space self-consistent-field (CASSCF) method.[16−18] The electronic coupling for the electron transfer reaction is calculated with the generalized Mulliken−Hush method.[19,20] The solvation properties such as the solvated free energies of reaction and the solvent reorganization energies are calculated with the frequency-resolved cavity model (FRCM).[21,22] In addition to studying the radical anionic thymine−acrylamide complex in solution, we investigate the influence of neighboring DNA base pairs on this reaction.

II. Theory and Methods

The theoretical formulation for PCET utilized in this paper is based on the recently developed multistate continuum theory.[12−15] As mentioned previously, in this formulation the solvent is described as a dielectric continuum, the solute is represented by a multistate valence bond model, and the transferring hydrogen nucleus is treated quantum mechanically. For a reaction involving the transfer of one electron and one proton, the PCET reaction is represented by four valence bond (VB) states. The four VB states are labeled 1*a*, 1*b*, 2*a*, and 2*b*,

† Part of the special issue "John C. Tully Festschrift".

* To whom correspondence should be addressed. E-mail: shs@chem.psu.edu.

10.1021/jp0209392 CCC: $22.00
Published on Web 06/27/2002

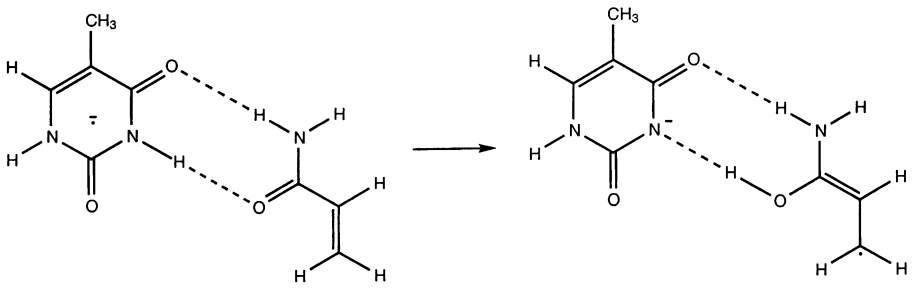

Figure 1. Schematic illustration of the PCET reaction in the radical anionic thymine−acrylamide complex.

where the label 1 or 2 indicates the electron transfer (ET) state and the label *a* or *b* indicates the proton transfer (PT) state. For the thymine−acrylamide system studied in this paper, the four VB states are as follows:

$$\begin{aligned}
&(1a)\quad [\mathrm{ThyNH}]^{-}\cdots[\mathrm{OAcr}]\\
&(1b)\quad [\mathrm{ThyN}]^{2-}\cdots{}^{+}[\mathrm{HOAcr}]\\
&(2a)\quad [\mathrm{ThyNH}]\cdots{}^{-}[\mathrm{OAcr}]\\
&(2b)\quad [\mathrm{ThyN}]^{-}\cdots[\mathrm{HOAcr}]
\end{aligned} \tag{1}$$

Note that states 1*a* and 2*b* correspond to the reactant and product, respectively, in Figure 1.

As shown in ref 12, the free energy surfaces for PCET reactions may be calculated as functions of two collective solvent coordinates, z_p and z_e, corresponding to PT and ET, respectively. The ET diabatic free energy surfaces corresponding to ET states 1 and 2 are calculated as mixtures of the *a* and *b* PT states. The reactants (**I**) are mixtures of the 1*a* and 1*b* diabatic states, and the products (**II**) are mixtures of the 2*a* and 2*b* diabatic states. The proton vibrational states are calculated for both the reactant (**I**) and product (**II**) ET diabatic surfaces, resulting in two sets of two-dimensional vibrational−electronic free energy surfaces that may be approximated as paraboloids. Electronically nonadiabatic PCET reactions are described in terms of nonadiabatic transitions from the reactant (**I**) to the product (**II**) ET diabatic vibrational−electronic surfaces. Electronically (and vibrationally) adiabatic PCET reactions are described in terms of the evolution along the ground vibrational−electronic surface comprised of a mixture of the reactant and product ET diabatic surfaces. Rate expressions have been derived in these two limits.[12,13] (Note that the dielectric continuum treatment of the solvent neglects hydrogen bonding between the solvent and solute, as well as dynamical properties of the solvent. Explicit solvent molecules may be included using a recently developed molecular dynamics approach for PCET.[23])

Within the framework of the multistate continuum theory,[12] the calculation of the free energy surfaces requires the gas phase valence bond matrix elements and the outer-sphere (solvent) reorganization energy matrix elements. The gas phase valence bond matrix elements are represented by molecular mechanical terms fit to electronic structure calculations or experimental data. The outer-sphere reorganization energy matrix elements are calculated with an electrostatic dielectric continuum model. As discussed in ref 13, inner-sphere (solute) reorganization energy may also be included. For the application presented here, however, the inner-sphere reorganization is neglected.

In this paper, the gas-phase valence bond matrix elements are based on a five-site linear model for the thymine−acrylamide complex:

$$\mathrm{D_e{-}N{-}H{-}O{-}A_e}$$

The electron donor, D_e, and acceptor, A_e, represent the approximate centers of thymine and acrylamide, respectively. The distances within this five-site model were determined by the optimized neutral geometry. The diagonal matrix elements are expressed as

$$\begin{aligned}
(h_0)_{1a,1a} &= U_{\mathrm{NH}}^{\mathrm{Morse}} + U_{\mathrm{OH}}^{\mathrm{rep}} + U_{1a}^{\mathrm{Coul}}\\
(h_0)_{1b,1b} &= U_{\mathrm{OH}}^{\mathrm{Morse}} + U_{\mathrm{NH}}^{\mathrm{rep}} + U_{1b}^{\mathrm{Coul}} + \Delta E_{1b}\\
(h_0)_{2a,2a} &= U_{\mathrm{NH}}^{\mathrm{Morse}} + U_{\mathrm{OH}}^{\mathrm{rep}} + U_{2a}^{\mathrm{Coul}} + \Delta E_{2a}\\
(h_0)_{2b,2b} &= U_{\mathrm{OH}}^{\mathrm{Morse}} + U_{\mathrm{NH}}^{\mathrm{rep}} + U_{2b}^{\mathrm{Coul}} + \Delta E_{2b}
\end{aligned} \tag{2}$$

(Note that the dependence of the matrix elements on the proton coordinate, r_p, is suppressed in eq 2 for clarity.) The Morse potential for an X−H bond of length, R_{XH}, is

$$U_{\mathrm{XH}}^{\mathrm{Morse}}(r_p) = D_{\mathrm{XH}}(1 - \mathrm{e}^{-\beta_{\mathrm{XH}}(R_{\mathrm{XH}}-R_{\mathrm{XH}}^{0})})^2 \tag{3}$$

and the repulsion term between nonbonded atoms X and H separated by distance R_{XH} is

$$U_{\mathrm{XH}}^{\mathrm{rep}}(r_p) = D'_{\mathrm{XH}}\,\mathrm{e}^{-\beta'_{\mathrm{XH}}R_{\mathrm{XH}}} \tag{4}$$

Here, the symbol X represents either nitrogen (N) or oxygen (O). The Coulomb interaction potential between the transferring H atom and the other sites is

$$U_i^{\mathrm{Coul}}(r_p) = \sum_k \frac{q_k^i q_{\mathrm{H}}\,\mathrm{e}^2}{R_{k\mathrm{H}}} \tag{5}$$

where $\sum_k$ is a sum over all sites except the transferring hydrogen and the atom bonded to the hydrogen, $R_{k\mathrm{H}}$ is the distance between the hydrogen atom and site *k*, q_{H} is the charge assigned to the hydrogen, and q_k^i is the charge on site *k* for diabatic state *i*. In this paper, the couplings are assumed to be constant:

$$\begin{aligned}
(h_0)_{1a,1b} &= (h_0)_{2a,2b} = V^{\mathrm{PT}}\\
(h_0)_{1a,2a} &= (h_0)_{1b,2b} = V^{\mathrm{ET}}\\
(h_0)_{1a,2b} &= (h_0)_{1b,2a} = V^{\mathrm{EPT}}
\end{aligned} \tag{6}$$

Within the framework of valence bond theory, V^{EPT} is expected to be significantly smaller than V^{ET} because V^{EPT} is a second-order coupling and V^{ET} is a first-order coupling. For simplicity, in this paper V^{EPT} was approximated as zero.

We used the generalized Mulliken−Hush (GMH) approach to calculate approximate values for the electronic coupling V^{ET}.[19,20] In this approach,[24] the electronic matrix element V_{if} between two *diabatic* electronic states *i* and *f* is expressed in

terms of the corresponding *adiabatic* state characteristics as

$$V_{if} = \frac{|\mu_{tr}|\Delta E_{ad}}{\sqrt{|\Delta\mu_{ad}|^2 + 4\mu_{tr}^2}} \quad (7)$$

where $\Delta\mu_{ad}$ is the difference in dipole moments, μ_{tr} is the transition dipole moment, and ΔE_{ad} is the energy splitting for the adiabatic states.

The solvent reorganization energies are calculated with the frequency-resolved cavity model (FRCM) developed by Newton, Rostov, and Basilevsky.[21,22] This approach allows for distinct effective solute cavities pertaining to the optical and inertial solvent response. The cavities are formed from spheres centered on all of the atoms. The two effective radii for the solute atoms are defined as $r_\infty = \kappa r_{vdW}$ and $r_{in} = r_\infty + \delta$, where r_{vdW} is the van der Waals radius, κ is a universal scaling factor, and δ is a constant specific to the particular solvent. As given in ref 22, $\kappa = 0.9$ and $\delta = 1.0$ for anions in water. The static and optical dielectric constants of water at 298 K are $\epsilon_0 = 78.4$ and $\epsilon_\infty = 1.78$.[22] All atoms of the complex are included for the calculation of the solvation properties. The charge density of each diabatic (i.e., valence bond) state is defined by assigning appropriate partial charges to all atoms. The reorganization energy matrix element between diabatic states *i* and *j* is determined by calculating the interaction of the charge density of state *i* with the dielectric continuum solvent response to the charge density of state *j*.

In this paper, the parametrization of the gas phase matrix elements and the atomic coordinates and charges used for the FRCM calculations are based on electronic structure calculations of the thymine−acrylamide complex. The geometries were optimized with DFT using the B3LYP functional[25−27] and the 6-31G* basis set. These calculations were performed with the Gaussian 98 program.[28] The energies of the ground and excited electronic states, as well as the electronic coupling, were calculated at the CASSCF level[16−18] with the same basis set using the GAMESS program.[29] The atomic charges were determined from a CHELPG calculation[30] with CASSCF/6-31G* using the Gaussian 98 program.[28]

We investigated the effect of including diffuse basis functions for these calculations. According to the criterion given in ref 31, the negative vertical electron affinity of the neutral thymine molecule calculated with B3LYP/6-31+G* suggests that the diffuse functions in the basis set might provide unreliable results. In addition, diffuse basis functions may not be appropriate for the calculation of solvation properties because the solvent is expected to restrict the electronic density for open-shell systems. From a practical standpoint, the diffuse basis functions resulted in difficulties choosing the physically relevant active space for the CASSCF calculations when the transferring proton is bonded to acrylamide. On the other hand, we found that the electronic excitation energies calculated with CASSCF were similar for the 6-31G* and 6-31+G* basis sets when the transferring proton is bonded to thymine. Considering all of these factors, we did not use diffuse basis functions for the calculations described below. (Note that recently Sevilla and co-workers also investigated the effects of different basis sets for DNA bases.[32])

III. Results and Discussion

To obtain a structure for the application of the multistate continuum theory, we optimized the geometry of the neutral thymine−acrylamide complex with DFT at the B3LYP/6-31G* level. The optimization was performed with C_s symmetry to maintain planarity of the structure and hence to maximize the electronic coupling between thymine and acrylamide. At this level of theory, the N−O proton donor−acceptor distance is 2.85 Å. The optimization of the neutral complex is consistent with the assumption that ET is faster than the geometry relaxation process. (For comparison, we also optimized the negatively charged complex and found that the N−O distance increased from 2.85 to 3.0 Å, but this different geometry does not alter the qualitative results of this paper.)

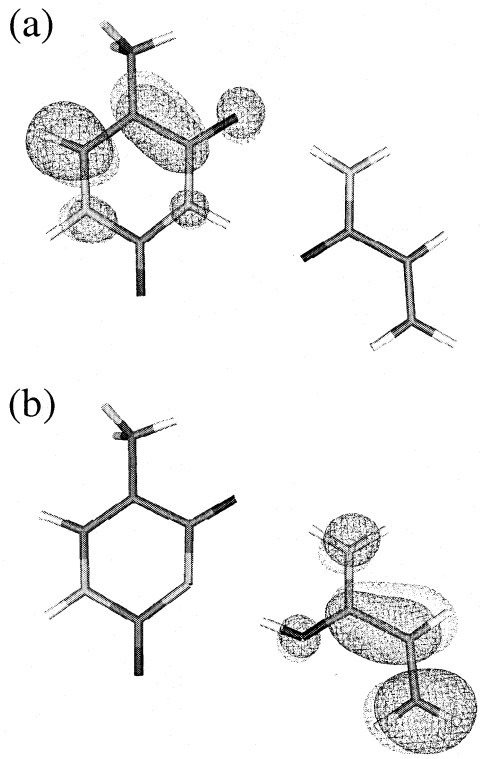

Figure 2. Singly occupied molecular orbitals (SOMOs) for the two proton-transfer states: (a) the proton is bonded to thymine; (b) the proton is bonded to acrylamide. Note that the SOMO is localized on thymine when the proton is bonded to thymine and is localized on acrylamide when the proton is bonded to acrylamide.

The matrix elements of the gas phase Hamiltonian were fit to electronic structure calculations of the gas phase radical anionic thymine−acrylamide complex. All solute nuclei except the transferring proton were assumed to be fixed to the optimized geometry for the neutral complex. We calculated the adiabatic energies with the state-averaged CASSCF/6-31G* method for a one-dimensional grid corresponding to the proton coordinate r_p. Nine electrons and eight molecular orbitals (MOs) were included in the active space; four of these MOs were localized on thymine, and four of these MOs were localized on acrylamide. The lowest two electronic states were equally weighted in the state-averaging process for the CASSCF calculations.

The singly occupied molecular orbitals (SOMOs) for the two PT states are depicted in Figure 2. This figure illustrates that the SOMO is localized on thymine when the proton is bonded to thymine and is localized on acrylamide when the proton is bonded to acrylamide. Note that these results are qualitatively different from previous DFT studies at the B3LYP/6-31+G* level.[7] In these previous studies, the unpaired spin density was found to be delocalized over both thymine and acrylamide when the proton is bonded to thymine and to be localized on acrylamide when the proton is bonded to acrylamide. We confirmed that the discrepancy between these two studies for the proton bonded to thymine is not due to the different basis sets. Specifically, we reproduced the delocalization over thymine

TABLE 1: Partial Charges for the Five-Site EVB Model

site	1*a*	1*b*	2*a*	2*b*
D_e	−0.8	−0.9	0.2	0.1
N	−0.6	−0.9	−0.7	−1.0
H	0.4	0.4	0.4	0.4
O	−0.7	−0.6	−0.6	−0.5
A_e	0.7	1.0	−0.3	0.0

TABLE 2: Parameters for the Five-Site Model Used to Describe the Gas Phase VB Hamiltonian Matrix Elements

D_{NH} (kcal/mol)	93
D_{OH} (kcal/mol)	102
β_{NH} (Å^{-1})	2.35
β_{OH} (Å^{-1})	2.35
R^o_{NH} (Å)	1.00
R^o_{OH} (Å)	0.96
D'_{NH} (kcal/mol)	2600
D'_{OH} (kcal/mol)	3000
β'_{NH} (Å^{-1})	2.5
β'_{OH} (Å^{-1})	2.5
ΔE_{1b} (kcal/mol)	52
ΔE_{2a} (kcal/mol)	0
ΔE_{2b} (kcal/mol)	36
V^{PT} (kcal/mol)	60
V^{ET} (kcal/mol)	0.8
V^{EPT} (kcal/mol)	0
D_e−N (Å)[a]	1.35
N−O (Å)[a]	2.85
O−A_e (Å)[a]	1.78

[a] Distances between sites.

and acrylamide with DFT at the B3LYP/6-31G* level and reproduced the localization on thymine at the CASSCF/6-31+G* level. In addition, we reproduced the localization of the SOMO on thymine at the MP2/6-31G* level[33−35] when the proton is bonded to thymine. Thus, we determined that the discrepancy between these two studies is due to the differences between the DFT and CASSCF methods.

We used the generalized Mulliken−Hush approach to estimate the electronic coupling between pairs of diabatic states. In this approach, the electronic coupling is estimated by eq 7. We calculated the electronic coupling for two different proton positions: (1) the proton bonded to thymine and (2) the proton in the center of the proton donor and acceptor. We obtained the energy splitting, ΔE_{ad}, and the transition dipole moment, μ_{tr}, between the relevant adiabatic electronic states, as well as $\Delta\mu_{ad}$, from CASSCF/6-31G* calculations with nine electrons and eight molecular orbitals in the active space (as described above). These calculations resulted in estimates of 0.7 and 0.8 kcal/mol for the reactant and central proton positions, respectively. Thus, we approximated the electronic coupling as V^{ET} = 0.8 kcal/mol. Note that this coupling is of similar magnitude as the thermal energy at room temperature, so this electron transfer reaction is in the intermediate regime between the electronically adiabatic and nonadiabatic limits.

The adiabatic electronic energy profiles were used to fit the parameters in the expressions given above for the gas phase Hamiltonian matrix elements. For the Coulomb interaction potential, the charges on the five sites were chosen to be consistent with the atomic charges calculated for the VB states with the CHELPG method.[30] These charges are given in Table 1. The parameters for the Morse potential and the β'_{XH} repulsion term were obtained from ref 36. The coupling V^{PT}, the ΔE_i parameters, and the D'_{XH} repulsion parameters were varied to fit the adiabatic electronic energy profiles. The values of the parameters are given in Table 2. A comparison of the electronic adiabatic states obtained from the CASSCF calculations and the four-state VB potential along the one-dimensional proton coordinate is provided in Figure 3.

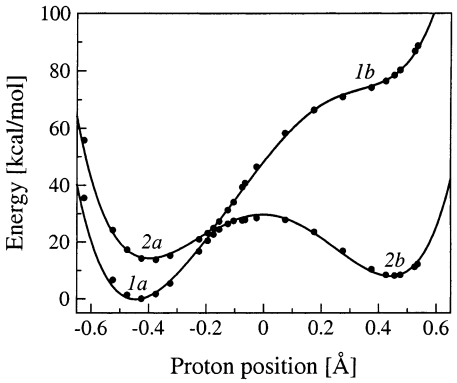

Figure 3. Energies of the gas phase adiabatic electronic states as functions of the proton coordinate. The symbols represent the CASSCF energies, and the solid line represents the VB potential. The minima of the curves are labeled according to the dominant VB state.

TABLE 3: Relevant Solvation Quantities[a,b] (kcal/mol) for Pairs of Diabatic VB States for the Thymine−Acrylamide Model with and without DNA

	Thy−Acr	DNA1−Acr[c] (full)	DNA1−Acr[c] (partial)
$\Delta G^{oPT}_{1a\rightarrow 1b}$	66.3	74.2	73.8
$\Delta G^{oET}_{1a\rightarrow 2a}$	6.6	19.6	20.8
$\Delta G^{oEPT}_{1a\rightarrow 2b}$	16.2	19.4	19.9
$\lambda^{PT}_{1a\rightarrow 1b}$	3.3	1.7	1.6
$\lambda^{ET}_{1a\rightarrow 2a}$	24.8	14.2	13.5
$\lambda^{EPT}_{1a\rightarrow 2b}$	10.7	5.8	5.5

[a] $\Delta G^o_{i\rightarrow j}$ denotes the free energy difference of solvated VB states *i* and *j*. [b] $\lambda_{i\rightarrow j}$ denotes the solvent reorganization energy between VB states *i* and *j*. [c] The DNA1 fragment model is described in the text. The results are given for both the partially and fully optimized structures.

We calculated the solvent reorganization energy matrix elements with the FRCM method. The atomic charges for each VB state were obtained from a CHELPG calculation[30] on the four VB states. In this case, the wave functions were calculated with the CASSCF method including one electron and two molecular orbitals (one localized on thymine and one localized on acrylamide) in the active space. For comparison, we also obtained a set of atomic charges for each VB state from a CHELPG calculation on the individual thymine and acrylamide fragments corresponding to each VB state using DFT at the B3LYP/6-31G* level. The solvent reorganization energy matrix elements calculated with the FRCM method were very similar using these two methods for obtaining atomic charges. This similarity indicates that the results are not sensitive to the details of the charge distributions.

As described in ref 37, these solvent reorganization energy matrix elements may be used to calculate the free energy differences and the reorganization energies for pairs of solvated VB states. Table 3 presents these quantities for the thymine−acrylamide system within the four-state VB model given in eq 1. As expected, the solvent reorganization is smaller for PT than for PCET and is larger for ET than for PCET. Additionally, although in the gas phase the 2*b* VB state is lower in energy than the 2*a* VB state, the solvated 2*a* state is lower in energy than the solvated 2*b* state. This observation suggests that the dominant charge transfer process in the gas phase would be EPT (i.e., both the electron and proton transfer) but the charge transfer process in solution would be ET (i.e., only the electron

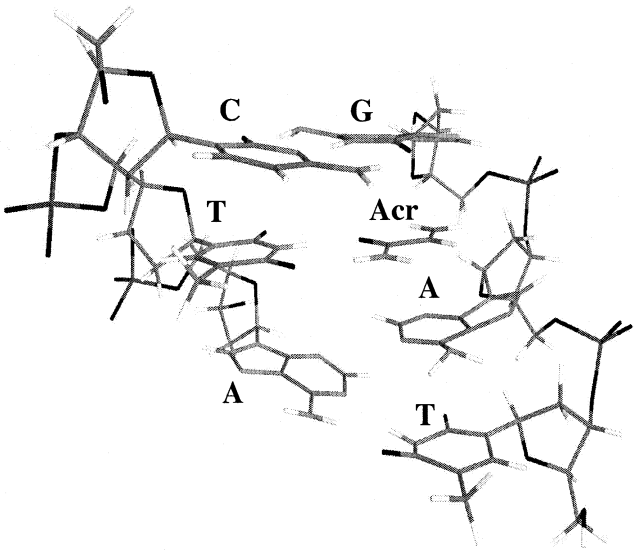

Figure 4. The DNA1−acrylamide complex optimized at the RHF/STO-3G level with the Onsager solvation model.

transfers). Here, EPT corresponds to a transition from a predominantly 1*a* state to a predominantly 2*b* state, while ET corresponds to a transition from a predominantly 1*a* state to a predominantly 2*a* state.

To investigate the influence of the DNA, we inserted the acrylamide into a DNA fragment composed of three base pairs. We investigated three DNA fragment models: DNA1 has the sequence 5′-CTA-3′, DNA2 has the sequence 5′-AAT-3′, and DNA3 has the sequence 5′-CTG-3′. The acrylamide was inserted to hydrogen bond to thymine and displace adenine in the middle base pair of each fragment. For all three fragments, we performed a full optimization of the fragment with the inserted acrylamide at the Hartree−Fock level with the STO-3G basis set using the Onsager continuum method[38,39] to account for the presence of solvent. In all three cases, the DNA structure opened up slightly because of the presence of the acrylamide and the lack of additional DNA bases to restrain the geometry of the fragment. To determine the effect of this structural change, we also investigated a partially optimized structure for each fragment model. For both the partially and fully optimized structures, we replaced the central thymine−acrylamide complex with the previously optimized geometry for consistency with the other multistate continuum theory calculations. (We found that the thymine−acrylamide complex maintained a nearly planar geometry during the optimization of the DNA fragments.) The three models exhibit very similar trends in the solvation properties, suggesting that the identity of the base pairs does not influence the qualitative results. We emphasize that these models are used to obtain only qualitative information and do not represent any specific biological systems. Figure 4 illustrates the fully optimized structure for the DNA1 fragment model.

We calculated the solvent reorganization energy matrix elements for these DNA systems using the FRCM method. For these calculations, the previously obtained atomic charges on the thymine−acrylamide complex were used and the other DNA atoms were assigned no charge. For comparison, we performed another calculation including atomic charges on the DNA obtained from a Mulliken analysis, and the results did not change significantly. This observation suggests that the dominant effect of the DNA fragment is the exclusion of solvent around the thymine−acrylamide complex. (Despite the limitations of the Mulliken analysis, it serves as a reasonable test of the sensitivity of the results to the detailed electrostatic potential on the DNA.)

Table 3 presents the free energy differences and the reorganization energies for pairs of solvated VB states for the partially and fully optimized DNA1 fragment model. The solvent reorganization energies for both structures are smaller than for the solvated thymine−acrylamide complex without DNA. For both structures, the solvated 2*b* state has similar but slightly lower energy than the solvated 2*a* state, indicating that the dominant charge transfer process will be EPT (i.e., both the proton and electron will transfer). The energy of the solvated 2*b* state relative to the solvated 2*a* state is lower for the more compact partially optimized DNA structure than for the fully optimized DNA structure.[40] These calculations indicate that the charge transfer process is qualitatively different in DNA than in pure solvent.

Figure 5 depicts the free energy profiles along the collective solvent coordinates and the proton potential energy curves with the corresponding proton vibrational wave functions for the solvated thymine−acrylamide and partially and fully optimized DNA1−acrylamide complexes. (The free energy surfaces are qualitatively similar for all three DNA fragment models.) For all systems discussed in this paper, the minimum of the reactant free energy profile is dominated by the 1*a* VB state, indicating that the electron is localized on thymine and the proton is bonded to thymine. Moreover, the proton vibrational wave function is localized in the proton potential energy well near thymine. For the solvated thymine−acrylamide complex, the minimum of the product free energy profile is dominated by the 2*a* VB state, indicating that the electron is localized on acrylamide and the proton is bonded to thymine. As for the reactant minimum, the proton vibrational wave function is localized in the proton potential energy well near thymine. Thus, the proton remains localized near thymine for both the reactant and product minima. In contrast, for the DNA1−acrylamide structures, the minimum of the product free energy profile is dominated by the 2*b* VB state,[41] indicating that the electron is localized on acrylamide and the proton is bonded to acrylamide. In this case, the proton vibrational wave function is localized in the proton potential energy well near acrylamide. This observation indicates that the proton transfers from thymine to acrylamide as the reaction progresses from the reactant to the product minimum.

As shown in Figure 5 parts b and c there is an avoided crossing between the lowest two product free energy surfaces for the DNA1−acrylamide structures. For both of these structures, the minimum of the product free energy surface is dominated by the 2*b* VB state. For the partially optimized DNA1−acrylamide structure, the product free energy surface is dominated by the 2*a* VB state for the lowest-energy intersection between the reactant and product free energy surfaces and is dominated by the 2*b* VB state for the second-lowest-energy intersection. For the fully optimized DNA1−acrylamide structure, the avoided crossing between the lowest two product free energy surfaces occurs at the intersection between the reactant and product free energy surfaces. For both systems, the detailed mechanism (i.e., the relative contributions of these product states during the reaction) depends on the potential energy surfaces, particularly the couplings between pairs of VB states. Regardless of the detailed mechanism, however, after vibrational relaxation, the final product state corresponds to the 2*b* state for both DNA1−acrylamide structures. These calculations illuminate the fundamental differences between the solvated thymine−acrylamide and the DNA−acrylamide models.

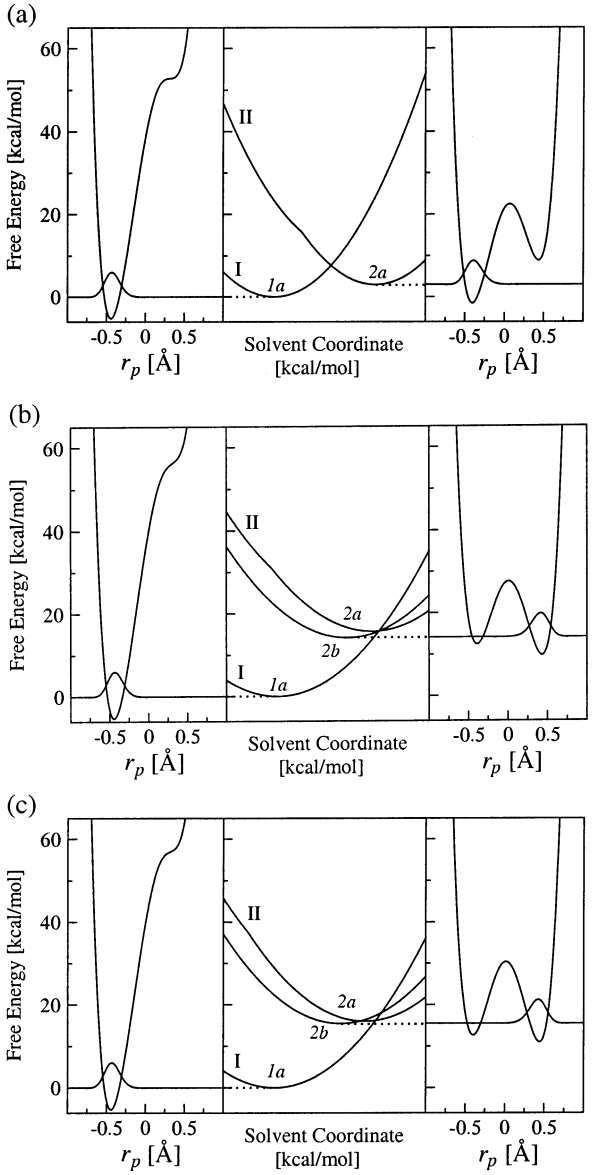

Figure 5. Analysis of the free energy surfaces for (a) the solvated thymine−acrylamide complex, (b) the fully optimized DNA1−acrylamide complex, and (c) the partially optimized DNA1−acrylamide complex. In the center frame are slices of the two-dimensional ET diabatic free energy surfaces as functions of the solvent coordinates. The slices were obtained along the line connecting the minima of the lowest energy reactant (**I**) and product (**II**) two-dimensional free energy surfaces. The lowest energy reactant (**I**) and product (**II**) free energy surfaces are included. (The lowest two product surfaces are included for panels b and c because they are very close in energy.) In the left frame is the reactant (**I**) proton potential energy curve and the corresponding proton vibrational wave function as a function of the proton coordinate, r_p, evaluated at the minimum of the ground state reactant free energy surface. In the right frame is the product (**II**) proton potential energy curve and the corresponding proton vibrational wave function as a function of the proton coordinate, r_p, evaluated at the minimum of the ground state product free energy surface.

IV. Conclusions

This paper presents the application of a multistate continuum theory for PCET to the radical anionic thymine−acrylamide complex. The ground and excited electronic states were calculated in the gas phase with the CASSCF/6-31G* method including nine electrons and eight molecular orbitals in the active space. At this level of theory, the SOMO is localized on thymine when the proton is bonded to thymine, and the SOMO is localized on acrylamide when the proton is bonded to acrylamide. The gas phase PCET product was found to be lower in energy than the gas phase ET product. Furthermore, on the basis of these CASSCF calculations, the electronic coupling for the ET reaction was calculated to be ∼0.8 kcal/mol with the generalized Mulliken−Hush method. This electronic coupling suggests that the ET reaction is in the intermediate regime between the electronically adiabatic and nonadiabatic limits.

The solvation properties of the thymine−acrylamide and the DNA−acrylamide complexes were calculated with the FRCM method. The solvent reorganization energies were found to be smaller in the DNA−acrylamide complex than in the thymine−acrylamide complex. Moreover, the solvated ET product was found to be lower in energy than the solvated PCET product for the thymine−acrylamide complex, whereas the solvated PCET product was found to be lower in energy than the solvated ET product for the DNA−acrylamide complex. These differences in solvation properties are due to a decrease in solvent accessibility in the presence of DNA.

The free energy surfaces were obtained as functions of two collective solvent coordinates. The proton potential energy curves and the corresponding proton vibrational wave functions were analyzed at the minima of the reactant and product free energy surfaces. These calculations indicate that the final product corresponds to single ET for the solvated thymine−acrylamide complex but to a net PCET reaction for the solvated DNA−acrylamide complex. These calculations illustrate that the balance between ET and PCET in the DNA−acrylamide system is highly sensitive to the solvation properties of the system.

Acknowledgment. We are grateful for financial support from NSF Grant CHE-0096357. S.H.-S. is the recipient of an Alfred P. Sloan Foundation Research Fellowship and a Camille Dreyfus Teacher-Scholar Award. C.C. is the recipient of a postdoctoral fellowship from the Swiss National Science Foundation.

References and Notes

(1) Steenken, S. *Chem. Rev.* **1989**, *89*, 503.
(2) Steenken, S. *Biol. Chem.* **1997**, *378*, 1293.
(3) Shafirovich, V.; Dourandin, A.; Huang, W.; Luneva, N. P.; Geacintov, N. E. *J. Phys. Chem. B* **1999**, *103*, 10924.
(4) Shafirovich, V.; Dourandin, A.; Luneva, N. P.; Geacintov, N. E. *J. Phys. Chem. B* **2000**, *104*, 137.
(5) Weatherly, S. C.; Yang, I. V.; Thorp, H. H. *J. Am. Chem. Soc.* **2001**, *123*, 1236.
(6) Colson, A.-O.; Besler, B.; Close, D. M.; Sevilla, M. D. *J. Phys. Chem.* **1992**, *96*, 661.
(7) Taylor, J.; Eliezer, I.; Sevilla, M. D. *J. Phys. Chem. B* **2001**, *105*, 1614.
(8) Cai, Z.; Li, X.; Sevilla, M. D. *J. Phys. Chem. B* **2001**, *105*, 10115.
(9) Razskazovskii, Y.; Roginskaya, M.; Sevilla, M. D. *Radiat. Res.* **1998**, *149*, 422.
(10) Paemel, C. V.; Frumin, H.; Brooks, V. L.; Failor, R.; Sevilla, M. D. *J. Phys. Chem.* **1975**, *79*, 839.
(11) Wilson, W. D. *Nucleic Acids in Chemistry and Biology*; Oxford University Press: New York, Tokyo, 1996.
(12) Soudackov, A. V.; Hammes-Schiffer, S. *J. Chem. Phys.* **1999**, *111*, 4672.
(13) Soudackov, A. V.; Hammes-Schiffer, S. *J. Chem. Phys.* **2000**, *113*, 2385.
(14) Hammes-Schiffer, S. Proton-Coupled Electron Transfer. In *Electron transfer in chemistry Vol. I. Principles, theories, methods, and techniques*; Balzani, V., Ed.; Wiley-VCH: Weinheim, Germany, 2001; pp 189−214.
(15) Hammes-Schiffer, S. *Acc. Chem. Res.* **2001**, *34*, 273.
(16) Roos, B. O.; Taylor, P.; Siegbahn, P. E. M. *Chem. Phys.* **1980**, *48*, 157.
(17) Cheung, L. M.; Sunberg, K. R.; Ruedenberg, K. *Int. J. Quantum Chem.* **1979**, *16*, 1103.
(18) Ruedenberg, K.; Schmidt, M. W.; Gilbert, M. M.; Elibert, S. T. *Chem. Phys.* **1982**, *71*, 41.
(19) Cave, R. J.; Newton, M. D. *Chem. Phys. Lett.* **1996**, *249*, 15.
(20) Cave, R. J.; Newton, M. D. *J. Chem. Phys.* **1997**, *106*, 9213.

(21) Basilevsky, M. V.; Rostov, I. V.; Newton, M. D. *Chem. Phys.* **1998**, *232*, 189.

(22) Newton, M. D.; Basilevsky, M. V.; Rostov, I. V. *Chem. Phys.* **1998**, *232*, 201.

(23) Kobrak, M. N.; Hammes-Schiffer, S. *J. Chem. Phys.* **2001**, *105*, 10435.

(24) Newton, M. D.; Cave, R. J. *Molecular Electronics*; Blackwell Scientific: Oxford, U.K., 1997.

(25) Becke, A. D. *J. Chem. Phys.* **1993**, *98*, 1372.

(26) Lee, C.; Yang, W.; Parr, R. G. *Phys. Rev. B* **1988**, *37*, 785.

(27) Pople, J. A.; Head-Gordon, M.; Fox, D. J.; Raghavachari, K.; Curtiss, L. A. *J. Chem. Phys.* **1989**, *90*, 5622.

(28) Frisch, M. J.; Trucks, G. W.; Schlegel, H. B.; Scuseria, G. E.; Robb, M. A.; Cheeseman, J. R.; Zakrzewski, V. G.; Montgomery, J. A., Jr.; Stratmann, R. E.; Burant, J. C.; Dapprich, S.; Millam, J. M.; Daniels, A. D.; Kudin, K. N.; Strain, M. C.; Farkas, O.; Tomasi, J.; Barone, V.; Cossi, M.; Cammi, R.; Mennucci, B.; Pomelli, C.; Adamo, C.; Clifford, S.; Ochterski, J.; Petersson, G. A.; Ayala, P. Y.; Cui, Q.; Morokuma, K.; Malick, D. K.; Rabuck, A. D.; Raghavachari, K.; Foresman, J. B.; Cioslowski, J.; Ortiz, J. V.; Stefanov, B. B.; Liu, G.; Liashenko, A.; Piskorz, P.; Komaromi, I.; Gomperts, R.; Martin, R. L.; Fox, D. J.; Keith, T.; Al-Laham, M. A.; Peng, C. Y.; Nanayakkara, A.; Gonzalez, C.; Challacombe, M.; Gill, P. M. W.; Johnson, B. G.; Chen, W.; Wong, M. W.; Andres, J. L.; Head-Gordon, M.; Replogle, E. S.; Pople, J. A. *Gaussian 98*, revision A.6; Gaussian, Inc.: Pittsburgh, PA, 1998.

(29) Schmidt, M. W.; Baldridge, K. K.; Boatz, J. A.; Elbert, S. T.; Gordon, M. S.; Jensen, J. H.; Koseki, S.; Matsunaga, N.; Nguyen, K. A.; Su, S.; Windus, T. L.; Dupuis, M.; Montgomery, J. A. *J. Comput. Chem.* **1993**, *14*, 1347.

(30) Breneman, C. M.; Wiberg, K. B. *J. Comput. Chem.* **1990**, *11*, 361.

(31) Guerra, M. *J. Phys. Chem. A* **1999**, *103*, 5983.

(32) Li, X.; Cai, Z.; Sevilla, M. D. *J. Phys. Chem. A* **2002**, *106*, 1596.

(33) Head-Gordon, M.; Pople, J. A.; Frisch, M. J. *Chem. Phys. Lett* **1988**, *153*, 503.

(34) Frisch, M. J.; Head-Gordon, M.; Pople, J. A. *Chem. Phys. Lett* **1990**, *166*, 275.

(35) Frisch, M. J.; Head-Gordon, M.; Pople, J. A. *Chem. Phys. Lett* **1990**, *166*, 281.

(36) Warshel, A. *Computer Modeling of Chemical Reactions in Enzymes and Solutions*; John Wiley: New York, 1991.

(37) Soudackov, A. V.; Hammes-Schiffer, S. *J. Am. Chem. Soc.* **1999**, *121*, 10598.

(38) Kirkwood, J. G. *J. Chem. Phys.* **1934**, *2*, 351.

(39) Onsager, L. *J. Am. Chem. Soc.* **1936**, *58*, 1486.

(40) For some DNA−acrylamide fragment models, the solvated 2*b* state is slightly higher in energy than the solvated 2*a* state for the fully optimized structure because of a more open DNA structure. Nevertheless, the trend in the solvation properties is the same for all three DNA−acrylamide fragment models studied, and the biologically relevant DNA system is expected to have a more compact structure as a result of additional base pairs.

(41) In Figure 5, the product free energy surfaces are mixtures of the 2*a* and 2*b* VB states. Thus, the free energy differences between the lowest two product states in Figure 5 parts b and c are not the same as the values reported in Table 3 for the pure VB states.